Appl. Phys. A 79, 131–137 (2004)
DOI: 10.1007/s00339-003-2261-y

Applied Physics A
Materials Science & Processing

P. THOMAS[1]
E. NABIGHIAN[1]
M.C. BARTELT[2]
C.Y. FONG[1]
X.D. ZHU[1,✉]

An oblique-incidence optical reflectivity difference and LEED study of rare-gas growth on a lattice-mismatched metal substrate

[1] Department of Physics, University of California, Davis, CA 95616, USA
[2] Department of Chemistry and Materials Sciences, Lawrence Livermore National Laboratory, Livermore, CA 94550, USA

Received: 3 February 2003/Accepted: 16 June 2003
Published online: 16 September 2003 •

ABSTRACT We studied the growth of Xe on Nb(110) from 33 K to 100 K using a combination of low-energy electron diffraction and an in situ oblique-incidence optical reflectivity difference technique. We found that a hexagonal close-packed Xe film grows after a transition layer of three monoatomic layers thick is formed. The first two monolayers, influenced by both the interaction with the Nb substrate and the Xe–Xe interaction, lack long-range order. The third monolayer forms a bulk-like hexagonal close-packed structure. Subsequently a bulk-phase Xe(111) film grows in step-flow mode from 54 K down to 40 K. At 40 K, we observed a brief crossover to a layer-by-layer mode. At 33 K the growth proceeds in a kinetically limited multilayer or a three-dimensional island mode.

PACS 68.35.Fx; 68.35.Ja; 82.20.-w; 61.16.Ch

1 Introduction

Heteroepitaxy of thin crystalline films is one of the methods for fabricating heterostructured materials that underlie many existing and future device applications [1]. It also serves as a fertile ground for basic material physics research on interplay of various kinetic processes that occur during unit-cell formation (e.g. intralayer and interlayer mass transport and surface reactions) [2]. Heteroepitaxy is complicated as the growth quality is also subject to factors such as mismatch in lattice constant and electronic structure, symmetry frustration, and intermixing between host and guest materials. Most heteroepitaxy studies have been focused on the pseudomorphic growth of a guest material on a host substrate with a lattice constant close to that of the guest (roughly within 10 to 15%). A pseudomorphic growth persists up to a critical thickness beyond which the accumulated strain in the film becomes too large to further sustain such a growth [1–5]. Less has been done on growth over highly mismatched substrates where the critical layer is less than one-monolayer thick. The issue becomes whether one can still grow high-quality crystalline films with a transition layer of a few monoatomic layers to release the strain or to bridge the lattice mismatch and symmetry frustration.

✉ Fax: +1-530/752-4717, E-mail: xdzhu@physics.ucdavis.edu

In this regard, growth of rare gases on metals and semiconductors serves as a useful model [6]. Due to the distinct difference in atomic configurations, rare-gas atoms do not intermix with metallic or semiconductor substrates. Because rare-gas atoms on a flat surface tend to form a hexagonal close-packed structure, by choosing the lattice constant of a substrate or its terminating plane one can study how the effects of lattice mismatch and symmetry frustration are accommodated in growth of rare-gas thin films. This is the subject of this report. Specifically, we study the transition layer between a lattice-mismatched metal substrate and a (111)-oriented rare-gas film.

We investigate the growth of Xe on Nb(110) with a small miscut angle of 0.1°. Nb(110) is a lattice-mismatched template for growth of crystalline Xe films as the latter tend to form a (111)-terminated close-packed structure with a bulk-phase Xe–Xe separation of 4.34 Å. This is unlike the growth of rare-gas films on graphite(0001) and (111) and (100) faces of a few fcc metals, where the first monolayer of Xe forms an incommensurate hexagonal close-packed superlattice. The latter is rotated to best accommodate the misfit. On (110) faces of bcc metals such as Nb(110), Cr(110), and W(110), misfits are too large to stabilize a rotated hexagonal close-packed superlattice for the first Xe monolayer [6–8]. Although Xe forms a commensurate structure at low coverage of $\Theta_1 = 0.25$ (relative to substrate atom density) on Cr(110) and W(110) [9], at close to saturation coverage (with the area per Xe atom in the range of 17 Å^2), Engel et al. observed that Xe adatoms on W(110) form centered-rectangular superlattices instead of hexagonal close-packed structures [9]. The first centered-rectangular superlattice forms at $\Theta_2 = 0.3$ by compressing the $p(2 \times 2)$ superlattice along the [110] azimuth on W(110). The second, more densely packed, centered-rectangular superlattice forms at $\Theta_3 = 0.4$ by compressing the first centered-rectangular superlattice along the [001] azimuth. Since a hexagonal close-packed Xe monolayer would have a coverage of $\Theta_{\text{close-packed}} = 0.43$ on W(110), this means that the interaction of Xe with W(110) stabilizes a more loosely packed structure for the first Xe monolayer. On Nb(110) we have also observed the evidence of more loosely packed structures in the first and second monolayers of Xe. Such a double layer has a strong effect on the structure and growth kinetics of subsequent Xe layers.

2 Experimental procedures

The experiment is performed in an ultra-high-vacuum chamber with a base pressure below 1×10^{-10} Torr. The chamber is equipped with an Omicron rear-view LEED/AES (low-energy electron diffraction/Auger-electron spectroscopy) system. The LEED screen is imaged onto a 16-bit CCD detector so that the LEED intensity can be measured quantitatively. The Nb(110) substrate is cleaned by sputtering at room temperature with a 50%–50% mixture of Ar ions/Ne ions at 1 keV and subsequent thermal annealing at 900 °C for 10 min [10]. The AES measurement indicates that the Ar-Ne mixture is effective for removing both carbon and oxygen from the Nb(110) surface. We monitor the temperature using a type-K thermocouple spot welded to the side of the Nb(110) sample, with the reference junction in liquid nitrogen. We determined the offset in our thermocouple voltage measurement system by submerging the sample in liquid nitrogen. We subtract the offset value from subsequently measured thermocouple voltages, and use the difference to assign the sample temperature from the standard OMEGA table for type-K thermocouples without further correction. For Xe deposition, we back-fill the chamber with 99.999%-purity Xe gas and the partial pressure is monitored with an ionization gauge.

The chamber has an optical access so that we can perform oblique-incidence optical reflectivity difference (OI-RD) measurements to monitor the growth in situ [11]. We used this method in an earlier study of growth of a commensurate, hexagonal close-packed Xe film on Ni(111) where we observed the crossover from a three-dimensional island growth below 35 K to a layer-by-layer growth at and above 40 K [12]. The details of the oblique-incidence optical reflectivity difference setup have been described elsewhere [11, 12]. In essence, let $r_{p0} = |r_{p0}| \exp(i\Phi_{p0})$ and $r_{s0} = |r_{s0}| \exp(i\Phi_{s0})$ be the reflection coefficients for p- and s-polarized light at the wavelength $\lambda = 0.6328\,\mu$m from the substrate before deposition. And, let $r_p = |r_p| \exp(i\Phi_p)$ and $r_s = |r_s| \exp(i\Phi_s)$ be the reflection coefficients after a Xe film is deposited on the substrate. Let $\Delta_p \equiv (r_p - r_{p0})/r_{p0} = \delta \ln r_p$ and $\Delta_s \equiv (r_s - r_{s0})/r_{s0} = \delta \ln r_s$. We measure $\Delta_p - \Delta_s = \delta \ln(r_p/r_s)$ as follows. We pass a p-polarized He-Ne laser beam through a photoelastic modulator (PEM) that alters the beam polarization from p-polarized to s-polarized at a frequency of $\Omega = 50$ kHz. The polarization-modulated beam passes through a Pockels cell that produces a variable phase shift Φ_0 between the s- and p-polarization components of the beam before the latter is incident on the substrate through a strain-free window. The reflected beam, after exiting the vacuum chamber through another strain-free window, then passes through an analyzer. The intensity of the beam $I_R(t)$ after the analyzer is detected with a photodiode. $I_R(t)$ consists of various harmonics of modulation frequency $\Omega = 50$ kHz. We measure the first and second harmonics, $I_R(\Omega = 50\,\text{kHz})$ and $I_R(2\Omega = 100\,\text{kHz})$, with lock-in amplifiers. It is easily shown that

$$I_R(\Omega) \sim I_{inc} \left| r_p r_s \cos\theta_A \sin\theta_A \right| \sin(\Phi_o + \Phi_p - \Phi_s)\,, \tag{1}$$

$$I_R(2\Omega) \sim I_{inc} \left(\left| r_p \cos\theta_A \right|^2 - |r_s \sin\theta_A|^2 \right)\,. \tag{2}$$

Here θ_A is the angle between the transmission axis of the analyzer and the p-polarization of the reflected beam. By adjusting θ_A before the deposition such that $\left|r_{p0}\cos\theta_A\right|^2 = |r_{s0}\sin\theta_A|^2$, and adjusting the variable phase shift Φ_o such that $\Phi_o + \Phi_{p0} - \Phi_{s0} = 0$, the subsequent changes in the first and second harmonics in response to the deposition of Xe are given by

$$\begin{aligned} I_R(\Omega) &\sim I_{inc} \left| r_{p0} \cos\theta_A \right|^2 \left[\left(\Phi_p - \Phi_{p0}\right) - \left(\Phi_s - \Phi_{s0}\right) \right] \\ &\sim I_{inc} \left| r_{p0} \cos\theta_A \right|^2 \mathrm{Im}\{\Delta_p - \Delta_s\}\,, \end{aligned} \tag{3}$$

$$\begin{aligned} I_R(2\Omega) &\sim I_{inc} \left| r_{p0} \cos\theta_A \right|^2 \left[\left| r_p/r_{p0} \right|^2 - |r_s/r_{s0}|^2 \right] \\ &\sim I_{inc} \left| r_{p0} \cos\theta_A \right|^2 \mathrm{Re}\{\Delta_p - \Delta_s\}\,. \end{aligned} \tag{4}$$

Experimentally we separately measure $I_{inc} \left| r_{p0} \cos\theta_A \right|^2$ so that, with (3) and (4), we extract $\Delta_p - \Delta_s = \delta \ln(r_p/r_s)$.

The reflectivity difference $\Delta_p - \Delta_s$ can be related to the morphology and optical properties of the deposited film through the classical three-phase model used by McIntyre and Aspnes [13]. In the limit that the average thickness $\langle d \rangle$ of the deposited film is much smaller than the wavelength of the probe laser λ, Zhu and coworkers have shown that [12, 14]

$$\begin{aligned} \Delta_p - \Delta_s \cong\, & -i \frac{4\pi \cos\varphi_{inc} \sin^2\varphi_{inc}\, \varepsilon_s \sqrt{\varepsilon_o}}{\lambda(\varepsilon_s - \varepsilon_o)\left[\varepsilon_s \cos^2\varphi_{inc} - \varepsilon_o \sin^2\varphi_{inc}\right]} \\ & \times \begin{bmatrix} \frac{(\varepsilon_{d,bulk} - \varepsilon_s)(\varepsilon_{d,bulk} - \varepsilon_o)(\langle d \rangle - d_0)}{\varepsilon_{d,bulk}} \\ + \frac{(\varepsilon_{d,terrace} - \varepsilon_s)(\varepsilon_{d,terrace} - \varepsilon_o) d_o}{\varepsilon_{d,terrace}} (1 - \theta_e) \\ + \frac{(\varepsilon_{d,edge} - \varepsilon_s)(\varepsilon_{d,edge} - \varepsilon_o) d_o}{\varepsilon_{d,edge}} \theta_e \end{bmatrix}\,. \end{aligned} \tag{5}$$

Here φ_{inc} is the incident angle from the medium with an optical dielectric constant ε_o. In our case the medium of incidence is vacuum with $\varepsilon_o = 1$. ε_s is the optical dielectric constant of the substrate. $\varepsilon_{d,bulk}$ is the bulk optical dielectric constant of the deposited material. $\varepsilon_{d,terrace}$ is the effective optical dielectric constant characterizing those surface atoms of the deposited material that are embedded in the flat terraces. $\varepsilon_{d,edge}$ is the effective optical dielectric constant of those surface atoms of the deposited material that are situated at step edges or kinks, which we loosely call 'step-edge atoms'. d_o is the thickness of one monolayer of the deposited atoms or molecules. θ_e is the fractional coverage of the step-edge atoms.

In homoepitaxy, $\varepsilon_{d,bulk} = \varepsilon_s$ and thus the first term on the right-hand side of (5) vanishes. In heteroepitaxy, the first term varies linearly with the average thickness $\langle d \rangle$ of the deposited material; the second and third terms combine to yield a term proportional to θ_e. In step-flow growth, θ_e remains constant and thus $\Delta_p - \Delta_s$ varies only with the thickness of the film. In layer-by-layer growth, θ_e varies periodically with the deposition of each monolayer [12]. As a result a small oscillatory component of $\Delta_p - \Delta_s$ adds on top of the $\langle d \rangle$-dependent, monotonic component. In three-dimensional growth or island growth, θ_e increases monotonically. Consequently, $\Delta_p - \Delta_s$ also varies monotonically but with a slope different from that for a step-flow growth.

We tested the usefulness of such a mean-field model as a quantitative probe by comparing the measured $\Delta_p - \Delta_s$ from one and two monolayers of compact xenon films on Nb(110) with the calculated value of the first term in (5). The

model reproduced both the incidence-angle dependence and the magnitude of the experimental $\Delta_p - \Delta_s$.

3 Results and discussion

In Fig. 1, we show $\mathrm{Im}\{\Delta_p - \Delta_s\}$ as a function of Xe exposure measured for different substrate temperatures. $\mathrm{Re}\{\Delta_p - \Delta_s\}$ behaves qualitatively the same. The Xe partial pressure during the deposition is $p = 1.4 \times 10^{-7}$ Torr and the reading has been corrected with the ionization factor for Xe. In Fig. 2, we show $\mathrm{Im}\{\Delta_p - \Delta_s\}$ obtained at 53 K during deposition at $p = 1.4 \times 10^{-7}$ Torr and after Xe is quickly evacuated from the chamber. Between 57 and 60 K, the coverage of Xe on Nb(110) increases linearly with exposure and reaches a plateau after 3.5 L (1 L $= 1.0 \times 10^{-6}$ Torr s). This corresponds to the formation of one 'full' monolayer of Xe. From the exposure, we find the sticking probability of Xe monomers on Nb(110) as $S_1 \sim 0.8$. Since the density of the first 'full' monolayer of Xe is less than that of a bulk-phase hexagonal close-packed structure as indicated by our LEED measurement, the sticking probability should be higher than 0.8. The first monolayer begins to desorb significantly at or above 75 K. When the substrate temperature is dropped below 57 K and yet is still above 54 K, the second monolayer forms on top of the first monolayer. At 54 K or below, the second layer is 'fully' formed after an exposure of 3.5 L. This means that the sticking probability onto the first monolayer is also close to unity. The change in the apparent adsorption rate between 54 and 57 K is due to a concurrent thermal desorption as illustrated in Fig. 2. Since the actual adsorption rate is the sum of the apparent adsorption rate and the desorption rate, we find that the sticking probability on the first Xe monolayer is roughly a constant between 54 and 57 K, i.e. $1 > S_2 > 0.8$.

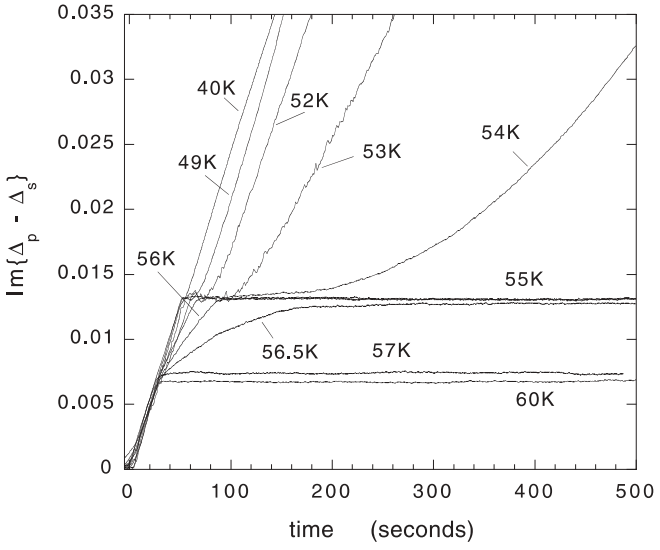

FIGURE 1 Optical reflectivity difference signal $\mathrm{Im}\{\Delta_p - \Delta_s\}$ vs. exposure time during Xe growth on Nb(110) from 40 K to 60 K. The Xe pressure is $p = 1.4 \times 10^{-7}$ Torr

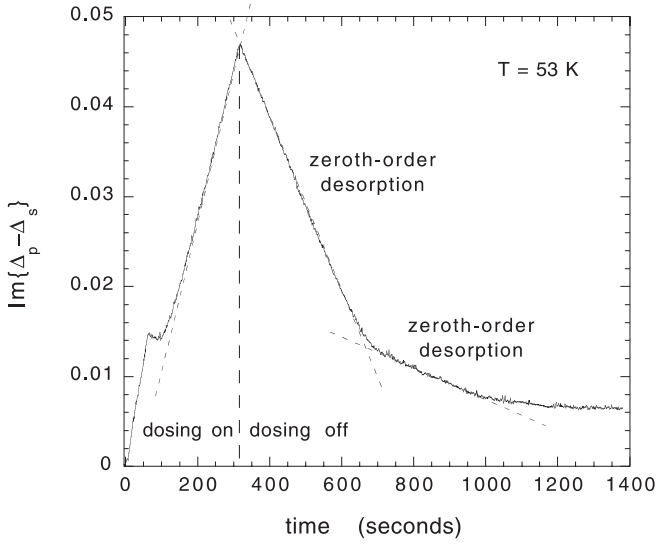

FIGURE 2 Optical reflectivity difference signal $\mathrm{Im}\{\Delta_p - \Delta_s\}$ during Xe growth on Nb(110) for a Xe pressure of $p = 1.4 \times 10^{-7}$ Torr, and after Xe is evacuated from the vacuum chamber. The desorption of the second monolayer and that of Xe overlayers on top of the third layer are both linear functions of time, or of zeroth order

Below 54 K, Xe begins to grow continuously on top of the first two monolayers (the double layer). Initially the rate of adsorption or growth on the double layer is very small. Once the third monolayer is formed, the growth of the subsequent layers is again a nearly linear function of exposure. At $T = 40$ K, the rate of change in $\mathrm{Im}\{\Delta_p - \Delta_s\}$ is the same as that during the growth of the second monolayer at 54 K. It means that the sticking probability of Xe atoms on the third monolayer and subsequent layers is again close to unity and the growth proceeds in a step-flow mode with $\theta_e \sim$ constant (according to (5)). Between 40 K and 54 K, the difference in the apparent growth or adsorption rate from those at 40 K is due to a concurrent thermal desorption (see Fig. 2). The sum of the thermal desorption rate and the apparent adsorption rate gives the actual adsorption rate in the absence of desorption, and it is roughly a constant from 40 to 54 K. As shown in Fig. 2, the isothermal desorption of Xe overlayers on top of the third monolayer is of zeroth order. The zeroth-order desorption is the result of phase coexistence of 2-D Xe solids and 2-D Xe gas between and on top of these 2-D solids. In this case the isothermal desorption rate remains constant as the 2-D Xe solids maintain a constant 2-D Xe gas 'pressure' or density, until the 2-D solids are completely consumed.

The Xe film structure as a function of exposure has been monitored with low-energy electron diffraction (LEED). Fig. 3a shows the LEED pattern of a clean Nb(110) substrate recorded at an electron energy of $E = 70$ eV. We focus on Xe overlayer structures at the completion of the first, second, and third monolayers on Nb(110). In contrast to the findings of Engel et al. [9], who observed well-resolved centered-rectangular superlattices for the first monolayer of Xe on W(110), we did not observe well-resolved spots that would indicate long-range-ordered structures. Instead we only observed a broad feature in the LEED pattern near the (0, 0) spot after the deposition of the first monolayer on Nb(110). To see the structure of this broad feature more clearly, we display in Fig. 3b the change in LEED pattern at the completion of the first monolayer recorded at an electron energy $E = 86$ eV. This was done by subtracting the LEED pattern of the clean substrate from the LEED pattern with the first

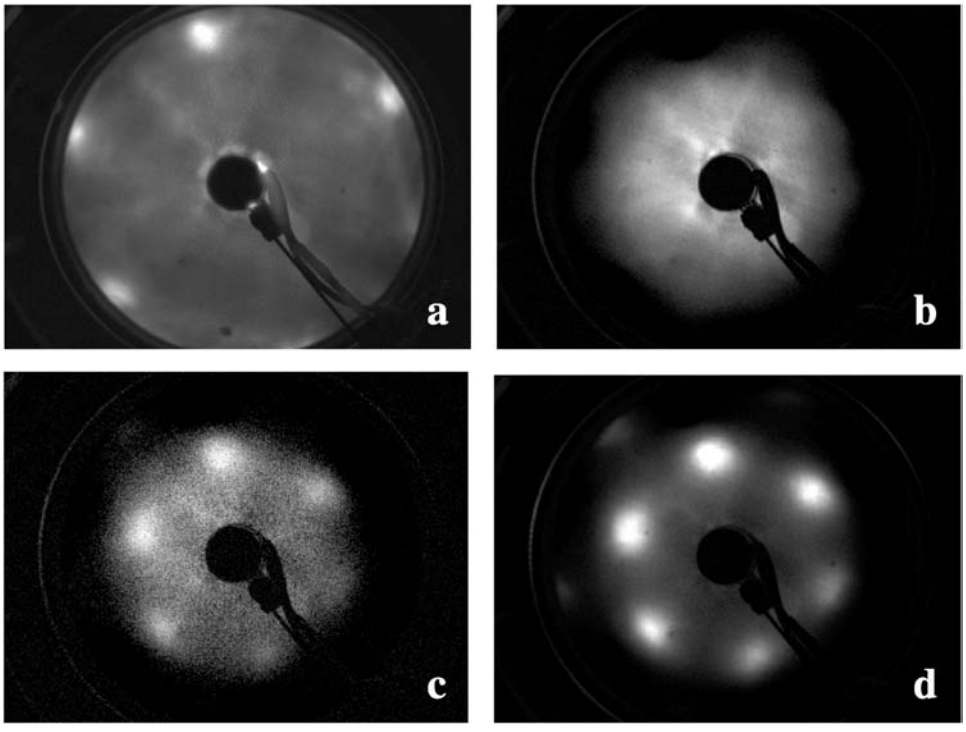

FIGURE 3 **a** LEED pattern recorded from clean Nb(110) (at $E = 70\,\text{eV}$); **b** change in LEED pattern recorded at $E = 86\,\text{eV}$ when a monolayer of Xe is adsorbed on Nb(110); **c** change in LEED pattern (at $E = 86\,\text{eV}$) when the third monolayer is formed on top of the second monolayer; **d** change in LEED pattern (at $E = 86\,\text{eV}$) when 10 monolayers of Xe are deposited on top of the third monolayer

monolayer Xe on the substrate. The two LEED patterns were measured under identical camera conditions including exposure time. The further change due to the deposition of the second monolayer is very similar to Fig. 3b. Fig. 3c shows the change in LEED pattern as a result of the formation of the third monolayer, obtained by subtracting the LEED pattern after deposition of the second monolayer from the LEED pattern after deposition of the third monolayer. Fig. 3d shows the additional change in LEED pattern after 10 more monolayers are grown on top of the third monolayer. The intensity of the (1, 0) spot from the Nb(110) substrate decreases exponentially with the thickness of the Xe overlayer with an exponent of $0.75\,\text{ML}^{-1}$.

Given that Engel et al. observed ordered superlattices of Xe on W(110) at close to saturation coverage [9], it is somewhat surprising that we did not observe a similar long-range-ordered structure in the first two monolayers of Xe on Nb(110), as evident from the absence of well-defined diffraction spots in Fig. 3b other than a broad distribution near the (0, 0) spot. The half-width of this broad distribution is less than the separation between the (0, 0) spot and the (1, 0) spot for a bulk-phase Xe(111) crystal. This shows that the average in-plane nearest-neighbor distance within the first two monolayers is less than the nearest-neighbor distance in bulk Xe crystal. Interestingly, the third monolayer forms a hexagonal close-packed structure that resembles the (111) plane of bulk-phase Xe. Beyond the third monolayer, the intensity of the (1, 0) spot corresponding to a (111)-oriented bulk-phase structure increases, indicating that a bulk-phase Xe(111) film grows on top of the third monolayer. The widths of the LEED spots were dominated by the limitation of our LEED setup instead of the domain sizes in the film. The azimuthal orientations of the third monolayer and subsequent layers are of Nishiyama–Wassermann (NW) type, where the fcc $[0\bar{1}1]$ row of the film is parallel to the bcc [001] azimuth on Nb(110) [15].

The preferential NW orientation indicates that the crystalline orientation of Nb(110) is felt by the third Xe monolayer through the first two monolayers and thus the latter must have a certain orientational ordering or preference. In Fig. 4, we show the real-space structure of a hexagonal close-packed structure of Xe on Nb(110) in the NW orientation. In Fig. 5 we reproduce three ordered structures of Xe on W(110) for comparison. It is instructive to notice that on W(110) the $p(2 \times 2)$ structure of Xe at low coverage progressively changes with increasing coverage by first compressing the superlattice along the [110] azimuth and then along the [001] azimuth, rather than along or perpendicular to the [111] or $[11\bar{1}]$ azimuth (the close-packed rows of W atoms). In fact, at high coverages, Xe close-packed rows continuously cross over the close-packed

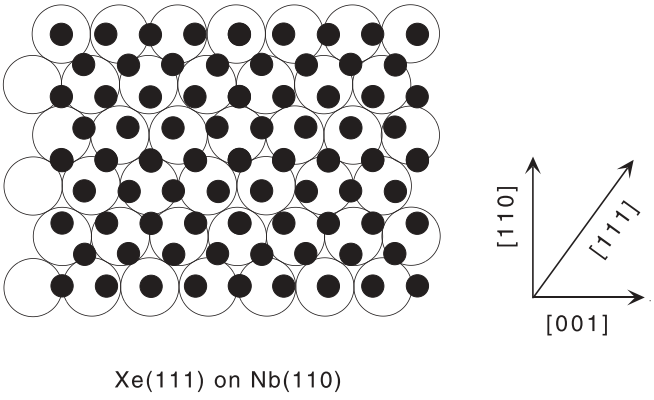

FIGURE 4 Hexagonal close-packed structure for the third Xe monolayer and the subsequent bulk-phase Xe(111) film in Nishiyama–Wassermann (NW) orientation on Nb(110) (*solid circles*)

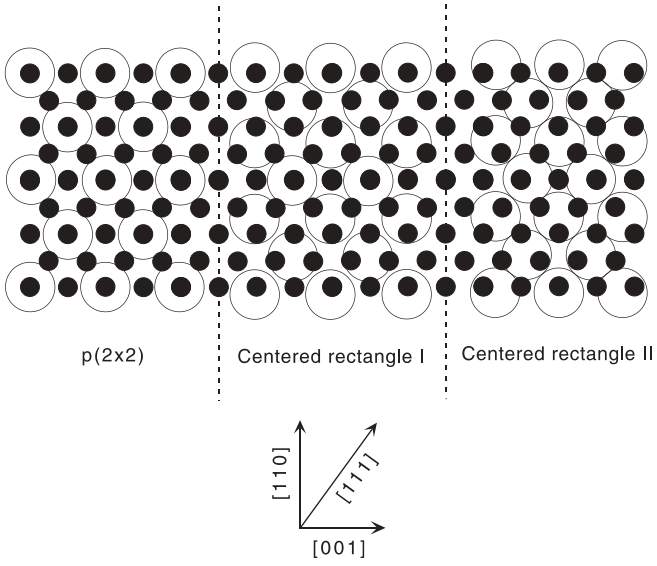

FIGURE 5 Three superlattices of Xe (*open circles*) on W(110) (*solid circles*) observed by Engel et al. [9] at different Xe coverages

rows of W atoms, indicating that the latter do not form deep troughs that would stabilize Xe rows. Instead, the [001] azimuth of W(110) is the direction along which rows of uncompressed and compressed Xe rows lay down and form the three observed superlattices. This suggests that the [001] azimuth on the (110) face of a bcc metal may be similar to the [110] azimuth on the (110) face of a fcc metal along which potential troughs form for adsorbed Xe. In this case one expects rows of Xe atoms to align along the [001] azimuth on W(110) and Cr(110), as observed. If this is also the case on Nb(110), we expect the first two Xe monolayers to consist of rows oriented along the [001] azimuth of Nb(110), even though well-defined LEED spots are absent. These oriented rows can further stabilize a hexagonal close-packed third monolayer in the NW orientation as shown in Fig. 4.

The apparent lack of long-range order in the first monolayer suggests that the Xe–Xe interaction energy and the binding energy corrugation on Nb(110) are comparable. We have performed a density-functional calculation of the binding energy for Xe on a frozen Nb(110) surface. We find that an isolated Xe atom prefers to adsorb at a low-coordination ontop site with a binding energy of 247 meV, similar to what Da Silva et al. found for Xe on Mg(0001), Al(111), Ti(0001), Cu(111), Pd(111), and Pt(111) [16]. The binding energies at short bridge sites and long bridges site are 196 meV and 177 meV, respectively [17]. The corrugation of the binding energy (50–70 meV), very close to the diffusion energy barrier $E_{\text{diff}} = 57$ meV for Xe on Nb(110) that we have separately measured using an optical diffraction technique [18], is comparable to the strength of three Xe–Xe bonds. As a result at 'full' coverage the first Xe monolayer may conceivably consist of domains of locally ordered superlattices oriented with rows of Xe atoms more or less along the [001] azimuth of the substrate. These locally ordered structures may include the high-coverage structures (see Fig. 5) for Xe on W(110). Since the lattice constant of Nb(110) is 4.4% larger that of W(110), the tendency for Xe to reside on low-coordination sites is expected to further distort these high-coverage structures. The combination of distorted, yet locally ordered Xe structures could lead to the poorly resolved LEED pattern as shown in Fig. 3b.

We now discuss the anomalous growth behavior for the third Xe monolayer, most noticeably at around 54 K as shown in Fig. 1. Unlike the adsorption of the first two monolayers and the layers beyond the third monolayer, the initial adsorption or growth rate on the double layer is nearly zero. The rate subsequently increases with the coverage towards the constant value characteristic of the growth on top of the third monolayer. This is particularly obvious at 54 K where an exposure of 20 L only leads to an increase in coverage of less than 0.1 ML on the double layer. Also, unlike the desorption of Xe multilayers beyond the third monolayer, the desorption of the third monolayer deviates from zeroth order when the coverage on the double layer becomes small (see Fig. 2 at around $t \sim 620$ s). Since the optical reflectivity difference signal reaches a plateau at the completion of the second monolayer over a wide range of substrate temperatures (between 40 and 56.5 K) and the second monolayer has a distinctly larger binding energy (or heat of desorption) as indicated in Fig. 2, the growth of the second monolayer must be completed before the third monolayer starts to form and, during the isothermal desorption, Xe atoms on top of the double layer leave first before the atoms in the second monolayer begin to desorb. This means that the double layer does not maintain the 2-D gas density on top of it at the expense of Xe atoms from within the double layer. As a result when the third monolayer is being depleted, it is expected that the desorption should deviate from that of zeroth order [6]. We note that even though the equilibrium between 2-D solids and 2-D gas explains the zeroth-order desorption and the constant adsorption rate for Xe multilayers on top of the third monolayer, it does not as simply explain why the rate of adsorption on the double layer increases with increasing coverage. Assuming that the sticking probability remains close to unity, the fact that the adsorption rate increases with increasing coverage implies that the desorption rate decreases accordingly. Under the 2-D equilibrium condition, we would then expect the isothermal desorption rate to increase as the third monolayer diminishes. This is not the case from the result shown in Fig. 2 at $t \sim 620$ s. In fact the desorption rate decreases as the third monolayer is being depleted.

One possible scenario that can lead to the anomalous growth behavior for the third monolayer is that the initial adsorption is kinetic-limited due to the peculiar structure of the double layer. Since the double layer is more loosely packed than in a Xe(111) crystal, the binding energy of Xe monomers (2-D gas) on the double layer is reduced. At 54 K, this can make the desorption rate of Xe monomers significantly larger than that from a close-packed Xe(111) crystal so that the initial adsorption rate on the double layer is much smaller. Though short-lived, neighboring adsorbed monomers can form dimers, trimers, septamers, or even larger 2-D clusters that are energetically more stable against desorption (the binding energy is increased by one or a multitude of Xe–Xe bonds). The total adsorption rate thus has an extra term that is proportional to the probability of an impinging Xe atom to encounter a stable cluster or an adsorbed monomer. This

causes the adsorption rate to increase with the coverage on the double layer. As the 2-D clusters grow into large hexagonal close-packed islands at the expense of the exposed area of the double layer, the adsorption rate becomes progressively dominated by the adsorption rate on these large 2-D islands and thus continues to increase towards the adsorption rate characteristic of the subsequent layers (at same partial pressure and same substrate temperature). During isothermal desorption, on the other hand, the desorption of the third monolayer is governed by the 2-D equilibrium among the 2-D islands, the 2-D gas on top of them, and the different 2-D gas evaporated from the kinks of the 2-D islands onto the exposed double layer. As a result the rate smoothly crosses over from that for Xe multilayers before the 2-D islands become completely consumed to that of the first-order desorption of the remaining 2-D gas on the double layer. The latter diminishes as the density of the 2-D gas is reduced to zero by desorption.

It is conceivable that the formation of stable clusters on top of the double layer involves some reordering of the second monolayer so that the latter becomes more bulk-like. This would further increase the binding energy of a cluster towards what it is on bulk-phase Xe(111). Such a reordering would have to be local since we did not observe a noticeable reduction of the broad intensity pattern near the (0, 0) spot at the completion of the third monolayer, other than the appearance of extra LEED spots corresponding to the formation of a hexagonal close-packed structure. The notion of local reordering is appealing as during the reordering the tendency of Xe rows in the second monolayer to orient along the [001] azimuth of Nb(110) as imposed by the structure of the first monolayer will help to seed the Nishiyama–Wassermann (NW) orientation of the third monolayer. Furthermore the reordering will most likely require 2-D clusters on the double layer to reach a critical size before it takes place. This will impose a similar or even stronger kinetic limit on the initial growth rate than we have just proposed so that the growth rate on the third monolayer becomes significant only after an extended exposure.

In an earlier study of growth of a commensurate Xe(111) film on Ni(111), we observed that the growth beyond the third monolayer (where the influence of the Ni substrate is negligible) goes through a transition from a three-dimensional island mode at 35 K to a layer-by-layer mode at 40 K [12]. Park et al. observed similar growth behaviors of Xe on Cu(111) using scanning tunneling microscopy [19]. The transition was attributed to a dramatic increase in the critical radius (R_c) of two-dimensional (2-D) Xe islands for second-layer nucleation. In our present study, we have also observed the evidence of such a transition at around 40 K. In Fig. 6, we display the real part of the optical reflectivity difference, $\mathrm{Re}\{\Delta_p - \Delta_s\}$, taken at 40 K. If we examine the optical signal more closely, we notice a small oscillatory component that rides on top of the envelope. The small oscillation becomes more noticeable if we subtract the envelope portion of the signal (as also shown in Fig. 6). We fit $\mathrm{Re}\{\Delta_p - \Delta_s\}$ between 10 L and 80 L to a polynomial of degree two and use the polynomial as the envelope. The average amplitude of the oscillation is about 5% of that for a full monolayer. The low signal-to-noise ratio has distorted the expected smooth oscillation in $\mathrm{Re}\{\Delta_p - \Delta_s\}$. The small oscillation indicates that the growth at 40 K and up to 54 K is predominantly a step-flow growth. At 40 K, it is accompanied by a small component of layer-by-layer growth. At 33 K, we can no longer observe any oscillatory feature above the noise. At 49 K, though the oscillation is still noticeable, the average amplitude is reduced by more than one-half. This means that as the temperature is lowered through 40 K, the growth partly crosses over from a step-flow mode to a layer-by-layer mode and then quickly into a three-dimensional island mode at 33 K. Based on the result of our earlier kinetic Monte Carlo simulation [12], the incomplete transition from a step-flow mode to a layer-by-layer mode is expected on the 0.1°-miscut Nb(110) substrate with an average terrace width of $L_t = 1300$ Å or less due to random terrace-width fluctuations [12].

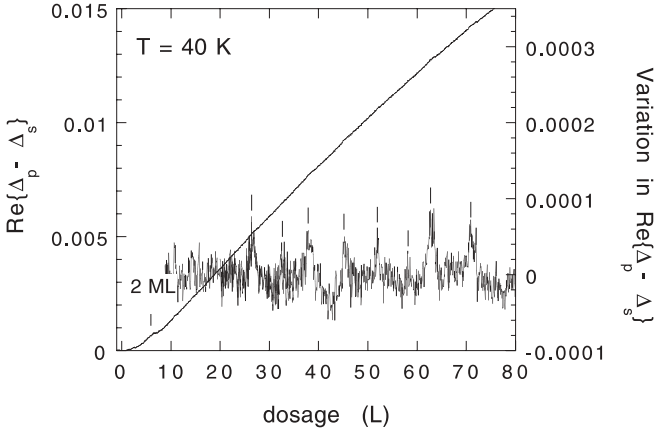

FIGURE 6 Optical reflectivity difference signal $\mathrm{Re}\{\Delta_p - \Delta_s\}$ vs. exposure during the Xe growth on Nb(110) at 40 K. The difference between the original signal and the envelope part of the signal (also shown) reveals small oscillations with exposure

4 Conclusion

To summarize, Xe growth on Nb(110) is a case where the critical thickness of a pseudomorphic overlayer is effectively zero. Unlike the growth of rare gases (Xe, Kr, Ar) on the basal plane of graphite where a hexagonal close-packed monolayer is formed and the misfit is compensated for by a rotation of the superlattice with respect to the substrate [20], Xe on Nb(110) represents a different way that a lattice mismatch is accommodated through the formation of a transition layer so that the subsequent growth of a bulk-phase crystalline film can be sustained. In this case the transition layer consists of two monolayers that lack long-range order, followed by an ordered hexagonal close-packed monolayer. The first two monolayers are strongly influenced by the substrate. The fact that the subsequent growth of a bulk-phase Xe(111) film proceeds in Nishiyama–Wassermann configuration suggests that Nb(110) has played a role of pinning down the orientation of the overlayer lattice through the first two monolayers, most likely by orienting the rows of Xe atoms in the double layer along the [001] azimuth of the substrate. It remains to be explored whether such a pinning effect applies to growth of other rare gases on Nb(110) and, likewise, to heteroepitaxy of fcc metals on (110) planes of a bcc metal substrate in general.

ACKNOWLEDGEMENTS X.D.Z. acknowledges the support of this work by NSF under Grant No. NSF-DMR-9818483, and in part

by the donors of the Petroleum Research Fund, administered by ACS. M.C.B. acknowledges the support by the Office of Basic Energy Sciences, Division of Materials Sciences of the US DoE under Contract No. DE-AC04-94AL85000.

REFERENCES

1 See, for example, W.K. Liu, M.B. Santos (Eds.): *Thin Films: Heteroepitaxial Systems* (Ser. Direct. Condens. Matter Phys. **15**) (World Scientific, Singapore 1999)

2 D.A. King, D.P. Woodruff (Eds.): *The Chemical Physics of Solid Surfaces*, Vol. 8 (Elsevier, Amsterdam 1997); J. Tersoff, A.W. Denier van der Gon, R.M. Tromp: Phys. Rev. Lett. **72**, 266 (1994)

3 T. Sakamoto, K. Sakamoto, K. Miki, H. Okumura, S. Yoshida, H. Tokumoto: In *Kinetics of Ordering and Growth at Surfaces* (NATO ASI Ser. **239**), ed. by M.G. Lagally (Plenum, New York 1990) p. 274; J.E. Macdonald, A.A. Williams, R. van Silfhout, J.F. van der Veen, M.S. Finney, A.D. Johnson, C. Norris: In *Kinetics of Ordering and Growth at Surfaces* (NATO ASI Ser. **239**), ed. by M.G. Lagally (Plenum, New York 1990) p. 473

4 G.J. Whaley, P.I. Cohen: Mater. Res. Soc. Symp. Proc. **160**, 35 (1990); N. Kuze, H. Goto, S. Miya, S. Muramatsu, M. Matsui, I. Shibasaki: Mater. Res. Soc. Symp. Proc. **399**, 165 (1996)

5 E. Bauer, H. Poppa, G. Todd, P.R. Davis: J. Appl. Phys. B **48**, 3773 (1977); E. Bauer, J.H. van der Merve: Phys. Rev. B **33**, 3657 (1986); E. Bauer: in [2], p. 46

6 P. Zeppenfeld: In *Physics of Covered Solid Surfaces*, Landolt-Börnstein, New Ser., Group III, Vol. 42: *Numerical Data and Functional Relationships in Science and Technology*, Subvol. A: *Adsorbed Layers on Surfaces* (Springer, Berlin 2001) pp. 67–95

7 C.G. Shaw, S.C. Fain, Jr., M.D. Chinn: Phys. Rev. Lett. **41**, 955 (1978); M.D. Chinn, S.C. Fain, Jr.: Phys. Rev. Lett. **37**, 146 (1977); J.A. Venables, H.M. Kramer, G.L. Price: Surf. Sci. **55**, 373 (1976); S. Calisti, J. Suzanne, J.A. Venables: Surf. Sci. **115**, 455 (1982)

8 A.D. Novaco, J.P. McTague: Phys. Rev. Lett. **22**, 1286 (1977)

9 T. Engel, P. Bornemann, E. Bauer: Surf. Sci. **81**, 252 (1979); T. Komeda, Y. Sakisaka, M. Onchi, H. Kato, S. Suzuki, K. Edamoto, Y. Aiura: Phys. Rev. B **40**, 3344 (1989)

10 Using a combination of LEED and the optical reflectivity difference as an in situ probe (see, for example, E. Nabighian, X.D. Zhu: Appl. Phys. Lett. **73**, 2736 (1998)), we found that annealing sputtered Nb(110) to 900 °C for a few minutes is sufficient to produce a smooth surface. The details of ion erosion and thermal annealing of Nb(110) will be reported elsewhere

11 A. Wong, X.D. Zhu: Appl. Phys. A **63**, 1 (1996); X.D. Zhu, H.B. Lu, Guo-Zhen Yang, Zhi-Yuan Li, Ben-Yuan Gu, Dao-Zhong Zhang: Phys. Rev. B **57**, 2514 (1998); X.D. Zhu, Weidong Si, X.X. Xi, Qi Li, Q.D. Jiang, M.G. Medici: Appl. Phys. Lett. **74**, 3540 (1999); X.D. Zhu, W. Si, X.X. Xi, Qidu Jiang: Appl. Phys. Lett. **78**, 460 (2001)

12 E. Nabighian, M.C. Bartelt, X.D. Zhu: Phys. Rev. B **62**, 1619 (2000)

13 J.D.E. McIntyre, D.E. Aspnes: Surf. Sci. **24**, 417 (1971)

14 X.D. Zhu: unpublished

15 J.H. van der Merve: In *Chemistry and Physics of Solid Surfaces*, Vol. 5, ed. by R. Vanselow, R. Howe (Springer, Berlin 1984) p. 365

16 J.L.F. Da Silva, C. Stampfl, M. Scheffler: Phys. Rev. Lett. **90**, 66 104 (2003)

17 C.Y. Fong, X.D. Zhu: unpublished

18 P. Thomas, J. Gray, X.D. Zhu: unpublished

19 J.-Y. Park, S.-J. Kahng, U.D. Ham, Y. Kuk, K. Miyake, K. Hata, H. Shigekawa: Phys. Rev. B **60**, 16 934 (1999)

20 J.L. Seguin, J. Suzanne, M. Bienfait, J.G. Dash, J.A. Venables: Phys. Rev. Lett. **51**, 122 (1983)